Molecular beam epitaxy grown indium self-assembled plasmonic nanostructures

Ricky Gibson, Michael Gehl, Jasmine Sears, Sander Zandbergen, Nima Nader, Patrick Keiffer, Joshua Hendrickson, Alexandre Arnoult, Galina Khitrova

Molecular beam epitaxy grown indium self-assembled plasmonic nanostructures

Ricky Gibson [a,n], Michael Gehl [a], Jasmine Sears [a], Sander Zandbergen [a], Nima Nader [a,b,c], Patrick Keiffer [a], Joshua Hendrickson [b], Alexandre Arnoult [d], Galina Khitrova a

[a] College of Optical Sciences, University of Arizona, 1630 E University Blvd., Tucson, AZ 85721, USA
[b] Air Force Research Laboratory, Sensors Directorate, 2241 Avionics Circle, Wright-Patterson AFB, OH 45433, USA
[c] Solid State Scientific Corporation, 12 Simon St. Nashua, NH 03060, USA
[d] LAAS-CNRS, 7 Avenue du Colonel Roche, 31000, Toulouse, France

Abstract

We describe molecular beam epitaxy (MBE) growth conditions for self-assembled indium nanostructures, or islands, which allow for the tuning of the density and size of the indium nanostructures. How the plasmonic resonance of indium nanostructures is affected by the island density, size, distribution in sizes, and indium purity of the nanostructures is explored. These self-assembled nanostructures provide a platform for integration of resonant and non-resonant plasmonic structures within a few nm of quantum wells (QWs) or quantum dots (QDs) in a single process. A 4× increase in peak photoluminescence intensity is demonstrated for near-surface QDs resonantly coupled to indium nanostructures.

Keywords

A1. Nanostructures
A3. Molecular beam epitaxy
B1. Metals
B2. Semiconducting III–V materials

1. Introduction

The field of plasmonic nanostructures, where small volume structures can enhance electromagnetic fields that can be coupled to semiconductor quantum confined gain medium, is an expanding area of research. It has been shown that MBE grown silver films have improved optical constants, i.e. closer to intrinsic values, over e-beam or physical vapor deposited silver films [1]. This gives a possibility for improvements in the quality of plasmonic nanostructures or nano-antennas. It has also been shown that MBE can be used to grow site-controlled structures out of silver [2] and self-assembled structures with silver [3]and indium [4]. MBE growth allows for higher quality metallic nanostructures due to the improved optical constants and the self-

assembly creates a clean interface between the metallic nanostructure and semiconductor underneath. In the self-assembled case there is also no need for fabrication or post-processing for optical experiments, eliminating possible sources of impurities and contamination. By tuning the sizes of these nanostructures the resonant wavelength can be tuned [5] to be in resonance with QWs [6], [7] or QDs [8] just a few nanometers beneath the metallic structures. Growing these resonant indium islands in the same process as the semiconductor growth with MBE now opens up the possibility of encapsulating [9] the islands with more semiconductor material, including gain material. This would allow for larger coupling effects and possibly compensating metamaterial losses.

Here we present MBE growth conditions for indium islands, which allow for the tuning of the density, to well below 1 μm^{-2}, and size, from ~100 nm up to ~1.5 μm, of the indium islands. The larger island diameters are a result of a slow indium growth in the 1 ML/hr range, allowing for migration of the indium atoms throughout the growth.

2. Materials and methods

All samples have been grown on (100) GaAs wafers. The indium island samples have been grown in two different machines. The first is a Riber 32P where the sources are mounted on the rear vertical wall of the MBE growth chamber and aimed at the substrate which is mounted 25° from vertical, and 13° away from the most uniform growth position. In this chamber we have utilized 500 μm thick, double-side polished, two inch wafers cleaved into quarters for sample growth. These quarter wafers are held in three inch molybdenum substrate mounts (molyblocks) for quarter wafers with two tabs along the perpendicular sides. The other chamber used is a Riber 412 where the sources are mounted on the bottom of the MBE growth chamber and aimed at the substrate which is mounted horizontally in a five inch platen and the substrate is centered in the platen. In this chamber the growth is done on 350 μm thick, single-side polished, full two inch wafers which are n-doped with silicon (10^{-18} cm^{-3}). This chamber was used for all samples discussed below that have been grown with doped semiconductor layers. Both chambers utilize effusion cells with 7 N (7N5) purity indium in the Riber 32P (Riber 412).

After de-oxidizing the substrate, >400 nm of GaAs is grown at a substrate temperature of ~580 °C. For samples grown with InGaAs QWs or InAs QDs the substrate temperature is dropped to ~485 °C for the growth of these structures. The QW or QDs are then capped with between 3 and 10 nm of GaAs grown at the same substrate temperature. For the indium island growth the substrate temperature is lowered by cutting off the current to the substrate heater. At a substrate temperature of ~300 °C the arsenic flux is cut off. Once the arsenic flux is off, the substrate heater is set at a constant current and the substrate is allowed to come to an equilibrium

temperature, ~130 °C as measured with a type C thermocouple, while arsenic continues to be pumped out of the chamber. This time has been varied between 1 and 12 h. The indium island deposition then takes place with growth rates (beam equivalent pressure) between 0.27 ML/s (3.02×10^{-7} Torr) and 1 ML/hr or 0.00028 ML/s (3.97×10^{-10} Torr). In the latter case the indium cell temperature is only 60 °C above the standby temperature of the cell. The indium growth rate is given as the growth rate of InAs as calibrated from InAs QD growths.

Samples are characterized using atomic force microscopy (AFM), scanning electron microscopy (SEM), tunneling electron microscopy (TEM), energy dispersive x-ray spectroscopy (EDS), Fourier transform infrared (FTIR) transmission measurements, and photoluminescence (PL). By utilizing standard image processing techniques the sizes of the islands are extracted from AFM and SEM images.

3. Results

An interesting aspect of the indium island sample growths is the different distribution in island sizes achieved by the two different machines used. While there is expected to be small variations in substrate temperature and flux uniformity it is not expected that the indium islands grown in one chamber would have a Gaussian-like distribution in size while the other chamber would produce size distributions with a clear tail on the short side of the distribution. This is seen in Fig. 1(a) and (b) for the diameter of the indium islands along the (011) crystal axis and can be seen along the (0–11) crystal axis as well as in the height of the indium islands, although this is not shown here. The indium island samples with the tail in the distribution are grown on silicon doped GaAs but this is not expected to affect the formation of the indium islands in such a manner. In either case the standard deviation of the distribution is ~10% of the average size for both samples. Both distributions in Fig. 1 are developed by analyzing the diameter of over 850 islands for each sample. The distribution with the tail looks similar to the asymptotic distribution of the Lifshitz–Slyozov $t^{1/3}$ growth law [10] which is familiar to the growth of II–VI QDs in a glass matrix [11]. The tailed distribution shown in Fig. 1(b) has a much narrower peak than the $t^{1/3}$ distribution but still suggests diffusion of the indium islands is taking place and the larger islands are growing at the expense of the smaller islands. From the corresponding SEM images in Fig. 1(c) and (d) it can be seen that the indium islands tend to cluster for the Gaussian-like distribution of sizes and the samples showing the tail in the distribution seem to have some degree of order where they prefer to align together perpendicular to the (011) crystal axis (major flat) shown in upper right hand corner of Fig. 1(c). This direction is also parallel to the surface roughness of the sample seen on SEM images.

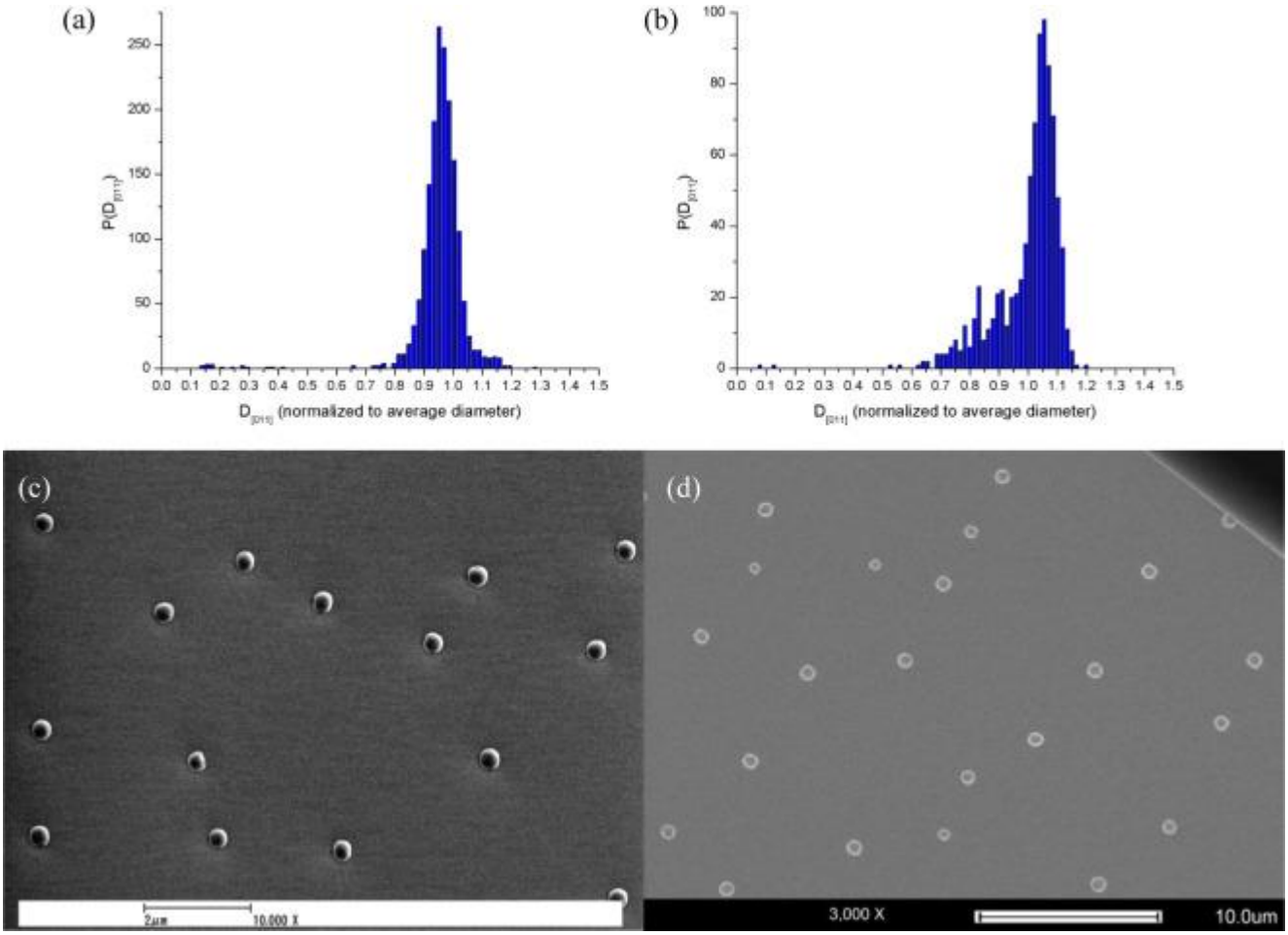

Fig. 1. Distribution of the diameter of the indium islands along the (011) crystal axis for a sample grown in the Riber 32 (a) and a sample grown in the Riber 412 (b). The distributions are scaled to their average diameter, which are 385 nm with a standard deviation of 34 nm and 834 nm with a standard deviation of 94 nm for samples shown in (a) and (b), respectively. (c) and (d) SEM images corresponding to the distributions in (a) and (b), respectively.

As discussed in the previous section, a wide range in growth rates or beam equivalent pressures are used, roughly a factor of 1000 between the highest and the lowest. By varying the growth rate and the amount of indium deposited the indium islands size can be varied between a diameter of 120 nm and a diameter of 1.5 μm, corresponding to heights of 50 nm and 445 nm. The densities achieved have been between 10 μm^{-2} and 0.007 μm^{-2}. Fig. 2shows plasmonic resonances, measured using FTIR, of several indium island samples along with corresponding SEM images for each sample. It is clear, that the larger islands have longer wavelength resonances and that a decrease in density of the indium islands decreases the collective transmission as measured by FTIR.

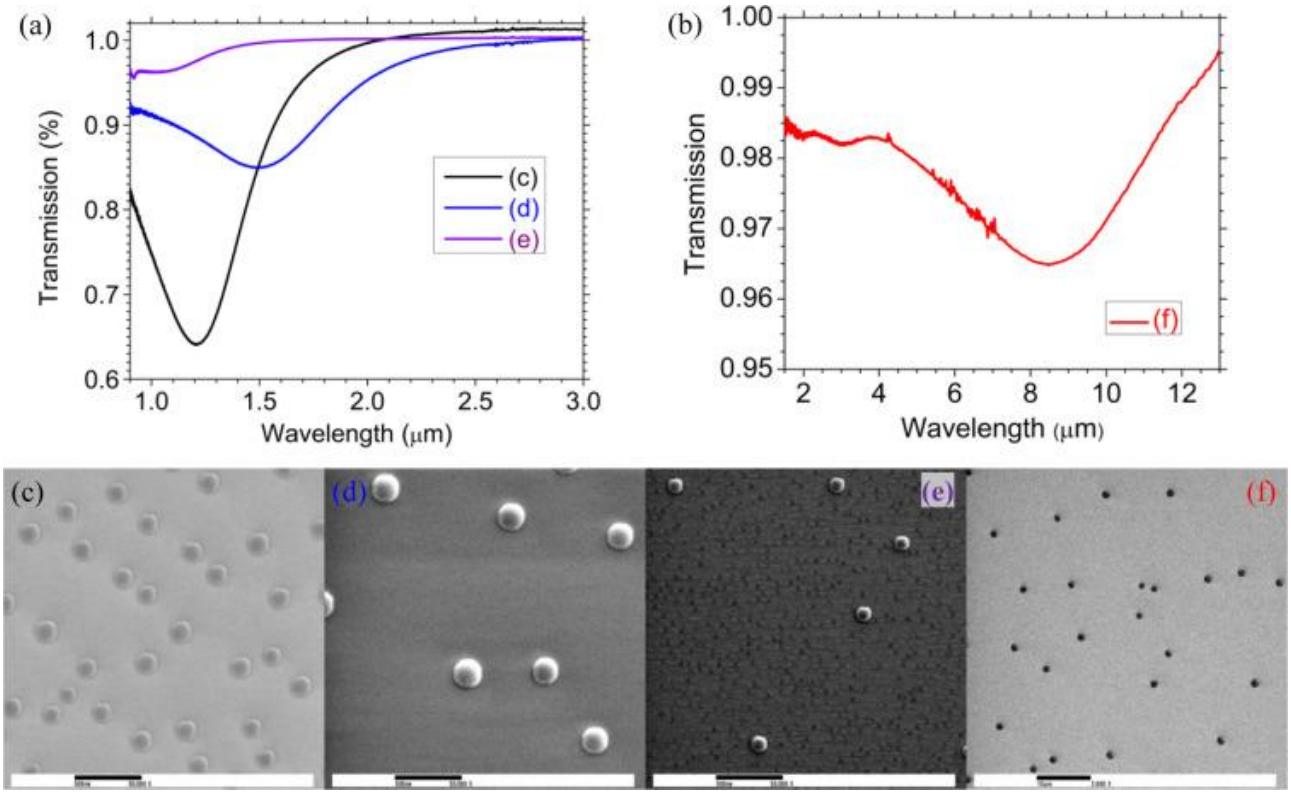

Fig. 2. (a) and (b) FTIR transmission measurements showing the plasmonic resonances of samples shown in the SEM images of (c), (d), (e), and (f). The scale bar in (c), (d), and (e) are 500 nm and in (f) is 10 μm.

Using EDS measurements the chemical composition of several indium islands on a single sample have been determined. Before the sample is prepared for TEM and EDS measurements the sample is coated with carbon and platinum to protect the sample during processing of the TEM slice. As shown in Fig. 3(a), a color map showing the indium (red), gallium (green), arsenic (violet), and oxygen (yellow) mapping of a single island, the indium islands are predominantly indium. A TEM of the island with the sample structure outlined is shown in Fig. 3(b). In the dashed outline in the central area of the indium island in Fig. 3(a), representing a 20 nm by 10 nm section of the island, the indium concentration was measured to be 89.9% with only 5.6% gallium and 4.5% arsenic. Despite the presence of gallium and arsenic in the islands and an oxide layer covering the island the samples show a strong plasmonic resonance as shown in Fig. 2.

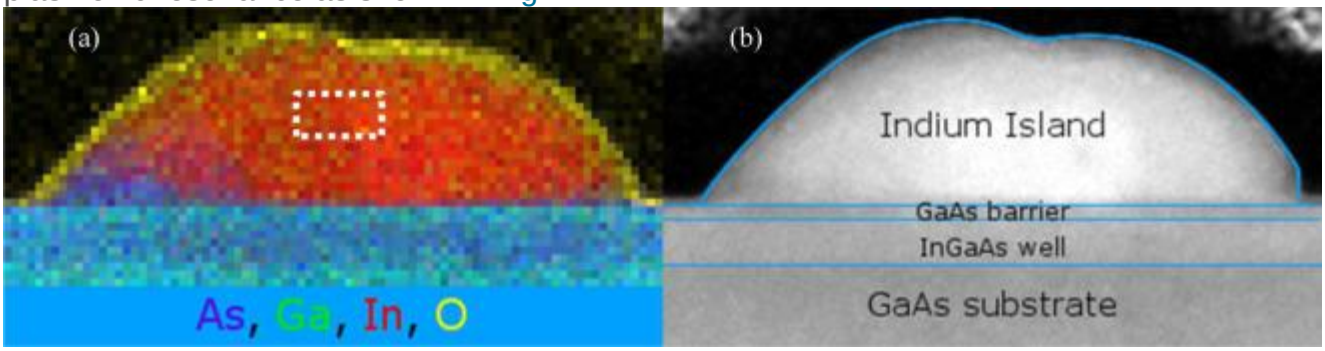

Fig. 3. (a) An EDS map of an island showing that it is predominantly indium (red) but also contains arsenic (violet), gallium (green), and oxygen (yellow). The white dashed box represents a 20 nm by 10 nm region where an indium concentration of 89.9% was measured. (b) A TEM image of the same island with the different regions of the structure outlined and labeled. (For interpretation of the references to color in this figure, the reader is referred to the web version of this article.)

As described above, the indium islands can be grown in close proximity to InAs QDs where the separation between the indium islands and the QDs can be precisely controlled by the thickness of the GaAs capping layer. In Fig. 4 we show a 4× increase in the peak intensity of the ensemble PL of InAs QDs when indium islands are present. The red data in Fig. 4 is from an InAs QD with a 7 nm GaAs cap but no indium islands. The black data is from a sample with similar InAs QDs and indium islands, at an island density of ~1 μm^{-2}, with a 7 nm GaAs cap separating the InAs QDs from the indium islands. For both samples the density of the QDs is ~80 μm^{-2} and the QD size is ~25 nm in diameter and ~3.5 nm tall. The shift in the PL peak to a shorter wavelength enhanced QDs is from the indium island resonance being centered at a shorter wavelength and enhancing the shorter wavelength QDs more. The PL measurements are done at a temperature of 10.8 K with above band pumping from a 632.8 nm continuous wave HeNe laser. About 1.6 mW of pump power is focused to a ~3 μm diameter spot, using a high NA 100× microscope objective. Also shown in Fig. 4 is the room temperature resonance of the indium islands, with dimension of 120 nm in diameter and 50 nm tall, as measured using an FTIR spectrometer. The resonance of the indium islands has been checked to not change between room temperature and 10 K but is not shown here.

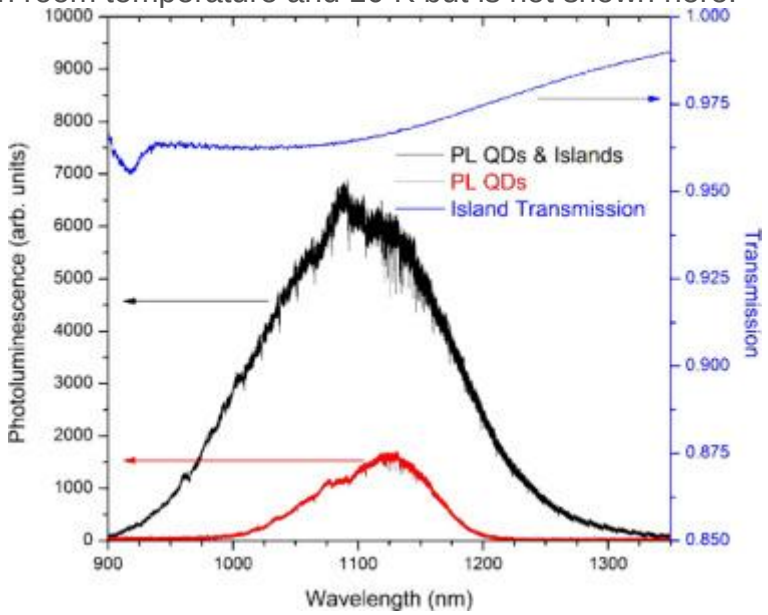

Fig. 4. PL of an indium island sample with 7 nm GaAs cap separating the InAs QDs and the indium islands (black), PL of just InAs QDs with a 7 nm GaAs cap (red), and

the transmission spectra of the indium islands (blue). PL measured at 10.8 K and transmission measured at room temperature. (For interpretation of the references to color in this figure, the reader is referred to the web version of this article.)

4. Conclusion

Self-assembled plasmonic nanostructures that can be grown in the same process as III–V quantum emitters have been explored and a wide range in sizes and densities has been demonstrated. A 4× increase in the peak PL of InAs QDs separated by 7 nm from the indium islands has been observed, demonstrating that the islands improve the luminescence of QDs and can in fact interact with them. This distance is less than the observed 1/*e* point, ~8 nm, of the coupling distance previously observed between a plasmonic structure and a QW [12] suggesting this is a useful platform to study coupling effects to III–V near-surface QDs. The increase in PL can be improved further by increasing the percentage of QD emission that is coupled to the plasmon mode [13] of on an indium island by controlling the position of the QDs relative to the plasmonic nanostructures or by using metals with lower losses as the plasmonic nanostructure [2]. An added interest of this platform is the ability to integrate superconducting structures, the indium islands, with III–V quantum emitters. The high indium concentration, up to ~90%, will be beneficial for any superconducting experiments or applications.

Acknowledgments

We gratefully acknowledge the use of facilities with the LeRoy Eyring Center for Solid State Science at Arizona State University. This work was funded by the Air Force Office of Scientific Research (AFOSR, Dr. Gernot Pomrenke, Grant FA9550-13-1-0003), the National Science Foundation Atomic, Molecular and Optical Physics (NSF-AMOP 1205031) and the Engineering Research Center for Integrated Access Networks (NSF ERC-CIAN, Award EEC-0812072). MG would like to acknowledge the support of the Department of Defense through the National Defense Science and Engineering Graduate (NDSEG) Fellowship Program. JS would like to acknowledge the support of Arizona Technology and Research Initiative Funding (TRIF). SZ would like to acknowledge the support of the Department of Energy (DOE) through the Office of Science Graduate Fellowship (SCGF) made possible in part by the American Recovery and Reinvestment Act of 2009, administered by ORISE-ORAU under Contract no. DE-AC05-06OR23100. JH would like to acknowledge support from the Air Force Office of Scientific Research (AFOSR, Program Manager – Dr. Gernot Pomrenke, Contract 12RY05COR). AA would like to acknowledge support from the French technology network RENATECH.

References

[1]
Y. Wu, C. Zhang, N.M. Estakhri, Y. Zhao, J. Kim, M. Zhang, X.-X. Liu, G.K. Pribil, A. Alù, C.-K. Shih, X. Li
Intrinsic optical properties and enhanced plasmonic response of epitaxial silver
Adv. Mater., 26 (35) (2014), p. 6106
[2]
A. Urbańczyk, R. Nötzel
Site-controlled Ag nanocrystals grown by molecular beam epitaxy—towards plasmonic integration technology
J. Appl. Phys., 112 (2012), p. 124302
[3]
Frank W.M. van Otten Adam Urbańczyk, Richard Nötzel
Self-aligned epitaxial metal-semiconductor hybrid nanostructures for plasmonics
Appl. Phys. Lett., 98 (24) (2011), p. 243110
[4]
A. Urbaczyk, G.J. Hamhuis, R. Nötzel
Coupling of single InGaAs quantum dots to the plasmon resonance of a metal nanocrystal
Appl. Phys. Lett., 97 (4) (2010), p. 043105
[5]
L. Novotny
Effective wavelength scaling for optical antennas
Phy. Rev. Lett., 98 (26) (2007), p. 266802
[6]
M. Gehl, S. Zandbergen, R. Gibson, M. Béchu, N. Nader, J. Hendrickson, J. Sears, P. Keiffer, MWegener, G. Kh itrova
Spectroscopic studies of resonant coupling of silver optical antenna arrays to a near-surface quantum well
J. Opt., 16 (11) (2014), p. 114016
[7]
N. Meinzer, M. Ruther, S. Linden, C.M. Soukoulis, G. Khitrova, J. Hendrickson, J.D. Olitzky, H.M. Gibbs, M. Wegener.
Arrays of Ag split-ring resonators coupled to InGaAs single-quantum-well gain
Opt. Express, 18 (23) (2010), p. 24140
[8]
A.G. Curto, T.H. Taminiau, G. Volpe, M.P. Kreuzer, R. Quidant, N.F. van Hulst.
Multipolar radiation of quantum emitters with nanowire optical antennas
Nature Commun., 4 (2013), p. 1750
[9]
C.R. Haughn, E.H. Steenbergen, L.J. Bissell, E.Y. Chen, K.G. Eyink, J.M.O. Zide, M.F. Doty
Carrier transfer from InAs quantum dots to ErAs metal nanoparticles
Appl. Phys. Lett., 105 (10) (2014), p. 103108
[10]
I.M. Lifshitz, V.V. Slyozov
The kinetics of precipitation from supersaturated solid solutions

J. Phys. Chem. Solids, 19 (1) (1961), p. 35

[11]

A.I. Ekimov

Optical properties of semiconductor quantum dots in glass matrix

Phys. Scr., 1991 (T39) (1991), p. 217

[12]

N. Meinzer, M. König, M. Ruther, S. Linden, G. Khitrova, H.M. Gibbs, K. Busch, M. Wegener

Distance-dependence of the coupling between split-ring resonators and single-quantum-well gain

Appl. Phys. Lett., 99 (11) (2011), p. 111104

[13]

A.V. Akimov, A. Mukherjee, C.L Yu, D.E. Chang, A.S. Zibrov, P.R. Hemmer, H. Park, M.D. Lukin

Generation of single optical plasmons in metallic nanowires coupled to quantum dots

Nature, 450 (2007), p. 402